Low Specific Contact Resistivity to n-Ge and Well-Behaved Ge n^+/p Diode Achieved by Implantation and Excimer Laser Annealing

2013 Appl. Phys. Express 6 106501

(http://iopscience.iop.org/1882-0786/6/10/106501)

Applied Physics Express 6 (2013) 106501
http://dx.doi.org/10.7567/APEX.6.106501

Low Specific Contact Resistivity to n-Ge and Well-Behaved Ge n^+/p Diode Achieved by Implantation and Excimer Laser Annealing

Chen Wang, Cheng Li*, Shihao Huang, Weifang Lu, Guangming Yan, Guangyang Lin, Jiangbin Wei, Wei Huang, Hongkai Lai, and Songyan Chen

Department of Physics, Semiconductor Photonics Research Center, Xiamen University, Xiamen, Fujian 361005, People's Republic of China
E-mail: lich@xmu.edu.cn

Received August 23, 2013; accepted September 5, 2013; published online September 24, 2013

Excimer laser annealing of phosphorus-implanted p-type germanium substrate with various laser energy densities for n^+/p junction were investigated. The effects of laser energy density on the redistribution of dopant, surface morphology, and recrystallization of the amorphous Ge induced by ion implantation were characterized. A low specific contact resistivity of $1.61 \times 10^{-6}\ \Omega\cdot cm^2$ was achieved from Al/n-Ge ohmic contact, in which phosphorus-implanted Ge was annealed at a laser energy density of $250\ mJ/cm^2$, tailoring a small phosphorus diffusion length, high activation level, and low dopant loss. A well-behaved Ge n^+/p diode with a rectification ratio up to 1.99×10^5 was demonstrated.

Germanium, chemically compatible with standard complementary metal–oxide–semiconductor (CMOS) technology, has attracted increasing attention due to its high carrier mobilities and large optical absorption coefficient at the wavelength for optical communication. Despite the significant progress in Ge MOSFET and photonic devices, there is still a big challenge in the fabrication of good ohmic contact on n-Ge.[1,2] On the one hand, a strong Fermi-level pinning effect on n-type Ge in the vicinity of the valence band maximum of Ge results in a high effective electron Schottky barrier height (SBH) when metals contact with n-Ge.[3,4] On the other hand, the fast diffusion of n-type dopants, which is positively related to the doping concentration, makes it difficult to achieve a high n-type doping level in Ge.[5,6] Both of them are obstacles to obtaining low specific contact resistivity for metal/n-Ge ohmic contacts and n^+/p shallow junctions.

Several approaches, such as furnace annealing,[7] rapid thermal annealing (RTA),[8] millisecond flash annealing[9] on n-type dopant ion-implanted Ge, have been attempted to obtain n^+Ge. However, these methods are accompanied by a significant dopant diffusion and poor electrical activation, as well as severe dopant loss. The fast diffusion and poor activation of n-type dopants are often ascribed to the vacancies in Ge, such as vacancy–impurity pairs, which act as acceptor states in the bandgap of Ge.[6] In situ doping of phosphorus during heteroepitaxial growth of Ge on Si also resulted in low doping concentration of less than $1 \times 10^{19}\ cm^{-3}$ due to the fast diffusion of phosphorus assisted by the defects or dislocations generated with the lattice mismatch between Si and Ge.[10,11] Because of these issues, contacts to n-Ge formed by standard processes are typically either rectifying or ohmic contacts with high resistivity ($>10^{-4}\ \Omega\cdot cm^2$).[12–14]

Compared with those annealing methods, excimer laser annealing (ELA) has unique advantages:[15] (1) Annealing time is only several tens of nanoseconds, much shorter than other annealing methods, resulting in minimal thermal diffusion of dopants and dopant loss; (2) ELA is a metastable process, allowing active dopant concentration beyond the dopant solid solubility limit; And (3) ELA can be used to selectively heat the specific regions of the device. ELA processes might provide a way to attain high activation levels and effectively suppress donor diffusion in Ge.[15,16] So far, there are a few reports on laser annealing for the formation of low-resistivity ohmic contacts to n-Ge[17,18] and high-rectification-ratio n^+/p shallow junction in Ge substrate.[16,19] It is desirable to clarify the effect of ELA on the dopant diffusion and electrical activation in Ge for its possible application in Ge device technology.

In this work, we investigated the effect of laser energy density on the phosphorus diffusion in Ge implanted with a high dose of $3.18 \times 10^{15}\ cm^{-2}$. A good ohmic contact was realized for Al contacting with phosphorus-implanted Ge annealed by excimer laser and Ge n^+/p junctions with high rectification ratio beyond 10^5 were achieved.

A Ga-doped p-type Ge(100) wafer with a resistivity of $0.088\ \Omega\cdot cm$ (doping concentration of $8 \times 10^{16}\ cm^{-3}$) was used as a substrate. The Ge wafer was circularly degreased in an ultrasonic bath of acetone and ethanol, immersed in hydrofluoric acid solution ($HF : H_2O = 1 : 50$) to remove the native oxide, rinsed with deionized water, and then finally blown dry by nitrogen. Prior to ion implantation, a 15 nm SiO_2 film was deposited on the Ge surface by plasma-enhanced chemical vapor deposition. Phosphorus was implanted at an energy of 30 keV and a dose of $3.18 \times 10^{15}\ cm^{-2}$. Before annealing, SiO_2 on the surface was removed using concentrated hydrofluoric acid at room temperature. Two-pulse laser annealing with various laser energy densities from 150 to $500\ mJ/cm^2$ was performed in nitrogen ambient using a 248 nm KrF excimer laser with a repetition frequency of 1 Hz and pulse duration of 25 ns. The laser spot size was $4 \times 3\ mm^2$, and continuous stepping in X- and Y-directions was carried out to cover the whole sample. The dopant profiles were measured by secondary-ion-mass spectrometry (SIMS), and the surface morphology and recrystallization of Ge were characterized by atomic force microscopy (AFM) and high-resolution transmission electron microscopy (HRTEM). The patterns of Al contacts for circular transmission line measurements (CTLM) and Ge n^+/p diodes were defined by standard photolithography and dry/wet etching with oxide hard masks. A 300 nm Al film was sputtered on the backside of the Ge wafer as the other electrode.

The phosphorus profile in Ge annealed using an excimer laser with various energy densities of 200, 300, and $500\ mJ/cm^2$ was measured by SIMS, as shown in Fig. 1. The peak concentration of phosphorus was $8.6 \times 10^{20}\ cm^{-3}$. After excimer laser annealing, the phosphorus profile can be

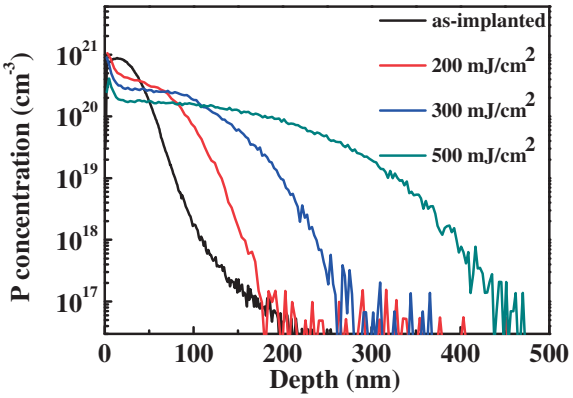

Fig. 1. Phosphorus SIMS depth profile of phosphorus-implanted Ge substrates before and after laser annealing at energy densities of 200, 300, and 500 mJ/cm^2 with two successive pulses.

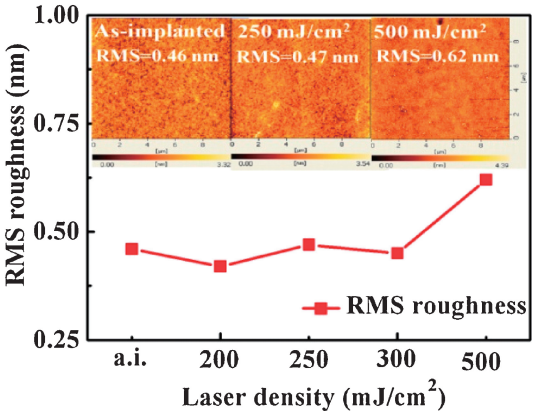

Fig. 3. RMS roughness measured by AFM as a function of laser energy density. The insets show the typical 10 × 10 μm^2 AFM images of the as-implanted and ELA samples.

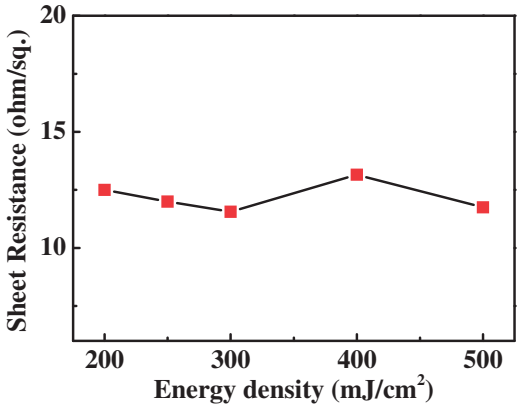

Fig. 2. Sheet resistance of phosphorus-implanted Ge as a function of laser energy densities from 200 to 500 mJ/cm^2.

well described with a plateau at the region of the peak concentration and the dopant diffusion toward the substrate at the region between 100 and 400 nm according to the laser energy density. From dose integration of the SIMS data of the ELA samples, we obtained a dose reduction of less than 10% for all the samples as compared with the implanted dose, which is much smaller than the reported results after other thermal treatments.[20–23] It can be seen that the phosphorus diffusivity in Ge increases with laser energy density in the range of 200 to 500 mJ/cm^2. The almost linear dependence of diffusivity on laser energy density makes it convenient to control the junction depth. Nevertheless, the diffusion of dopants is much less severe in Ge annealed by ELA than in that annealed by other thermal treatments such as rapid thermal annealing,[24] demonstrating that ELA is a promising annealing technique for shallow junction.

Figure 2 shows the sheet resistance of the phosphorus-implanted Ge after laser annealing with energy densities from 200 to 500 mJ/cm^2. The sheet resistance changes slightly with the increase of energy density, which is determined on the basis of the dopant profile $n(x)$ and junction depth X_j. Because the diffusion length increases with increasing laser energy density, the electrical concentration for the sample annealed at 200 mJ/cm^2 is the highest among them. Given that the phosphorus profile is approximated as a box shape, the average electrical activation concentration can be estimated using the equation,

$$R_S = \frac{1}{\int_0^{X_j} q\mu[n(x)][n(x) - N_B]\,dx},$$

where N_B is the background p-type doping concentration of the Ge wafer, and q is the electron charge. Using the mobility $\{\mu[n(x)]\}$ values,[25] the average electrical activation concentrations are evaluated to be 1.5×10^{20}, 1.2×10^{20}, and 6.0×10^{19} cm^{-3} for the samples annealed at 200, 300, and 500 mJ/cm^2, respectively, and the activation ratios are more than 80%. The maximum electrical concentration is close to the phosphorus solid solubility limit (2×10^{20} cm^{-3}).

The evolution of surface morphology of the samples after ELA was analyzed by AFM. Figure 3 shows the root-mean-square (RMS) surface roughness for the as-implanted and ELA samples. The insets are the typical AFM images after ELA with various energy densities. It can be seen that the surface is very smooth for all the samples. When the samples are annealed at a laser energy density of less than 300 mJ/cm^2, the RMS values are almost identical to that of the as-implanted sample (less than 0.5 nm). Even if the laser energy density is up to 500 mJ/cm^2, the surface roughness increases slightly to 0.62 nm.

Figure 4 shows the cross-sectional HRTEM images of the as-implanted and ELA samples at 200 and 500 mJ/cm^2. It is clearly seen that an amorphous Ge layer with the amorphous/crystal interface at 55 nm depth from the surface is formed, which is in good agreement with the prediction using the crystal damage energy density model with phosphorus implantation under 30 keV energy and in a dose of 3.18×10^{15} cm^{-2}.[26,27] After annealing at energy densities of 200 and 500 mJ/cm^2, the amorphous Ge layer is uniformly recrystallized, in which a few of defects can be detected.

In order to investigate the effects of laser energy density on the electrical properties of phosphorus-implanted Ge, the specific contact resistivity (ρ_C) of Al/n$^+$Ge contacts is measured with CTLM structures after the samples are annealed at 150, 200, and 250 mJ/cm^2. The relatively low laser energy densities of less than 300 mJ/cm^2 are chosen to

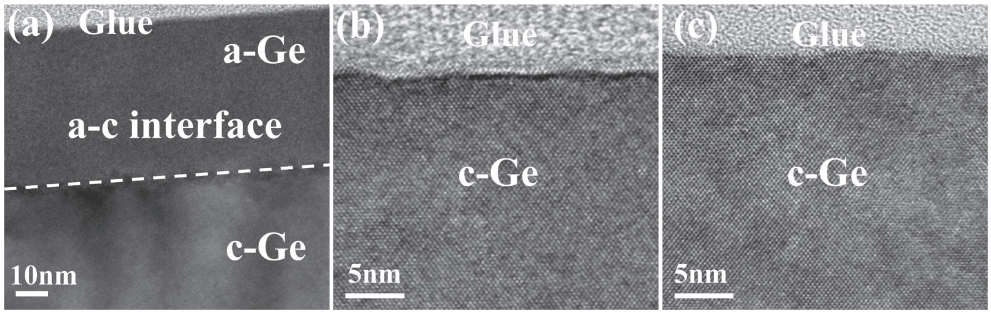

Fig. 4. Cross-sectional HRTEM images for (a) as-implanted Ge, (b) that laser annealed with 200 mJ/cm^2, and (c) that laser annealed with 500 mJ/cm^2.

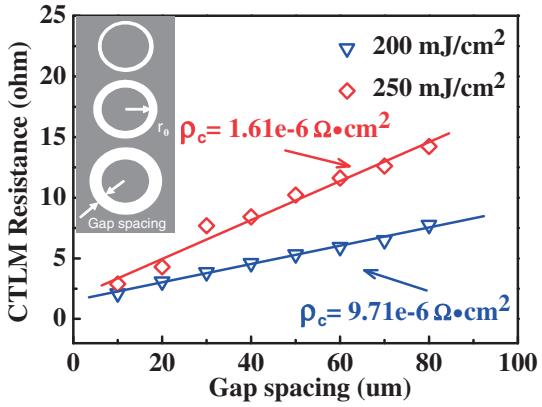

Fig. 5. Dependence of CTLM resistance on gap spacing for Al/n-Ge contacts. The inset shows the CTLM schematic structure (top view). A linear fit was used to extract the specific contact resistivity ρ_C.

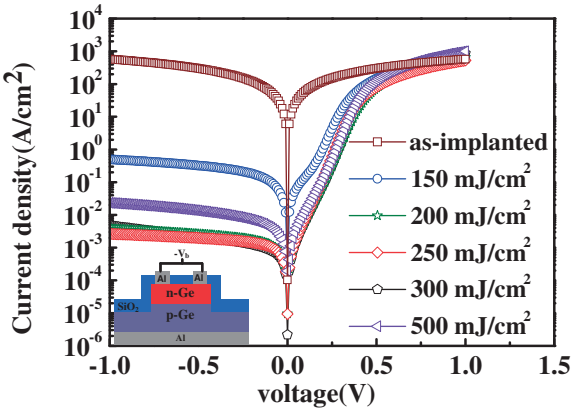

Fig. 6. I–V characteristics of Ge n$^+$/p shallow junction formed before and after ELA at laser energy fluences from 0 to 500 mJ/cm^2.

diminish the phosphorus diffusion depth. CTLM structures consist of a circular metal pad separated from a larger metal pad by a ring of semiconductor material with inner radius (r_0) of 80 µm and gap spacing from 10 to 80 µm. Applying a bias voltage between the two pads for different gap spacings to obtain the resistance, we can plot the resistance versus gap spacing and extract the sheet resistance R_S and transfer length L_T. The specific contact resistivity can be calculated as $\rho_C = R_S \cdot L_T{}^2$. Figure 5 shows the schematic of CTLM structures and the dependence of contact resistance for the samples annealed at 200 and 250 mJ/cm^2 on the gap spacing (for the sample annealed at 150 mJ/cm^2, the Al/n-Ge contact shows rectifying characteristics). The extracted values of ρ_C are about 9.71×10^{-6} Ω·cm^2 for the sample annealed at 200 mJ/cm^2 and 1.61×10^{-6} Ω·cm^2 for that annealed at 250 mJ/cm^2. Compared to our previous results,[13] the value of ρ_C is improved by about three orders of magnitude. This is a significant improvement compared to the typical values of $\rho_C \sim 10^{-4}$ Ω·cm^2 reported by other groups[12,14] for a single implantation followed by RTA, opening the opportunity to implement Ge in advanced CMOS and memory applications.

The typical current–voltage (I–V) characteristics of the Ge n$^+$/p junctions formed after ELA at laser energy densities from 0 to 500 mJ/cm^2 with two successive pulses are shown in Fig. 6. The extracted ideality factors from I–V characteristics of the n$^+$/p junctions after ELA at laser energy densities of 150, 200, 250, 300, and 500 mJ/cm^2 are about 1.44, 1.32, 1.28, 1.28, and 1.41, respectively. For the as-implanted samples, I–V characteristics are ohmic-like, which can be ascribed to the lower activation of phosphorus, being unable to compensate acceptors in the p-Ge, and large leakage current due to implantation damage. After ELA at 150 mJ/cm^2, the n$^+$/p junctions are formed, indicating that the n-type Ge layer is formed on the p-type Ge. The reverse current and ideality factors for the diodes decreases with increasing laser energy density from 0 to 300 mJ/cm^2, suggesting that the activation level of phosphorus and recovery of implant damage can be effectively improved by increasing energy density. However, when laser fluence is up to 500 mJ/cm^2, the ideality factor and reverse current density are increase, which could be attributed to the increased surface roughness and the lower doping level as confirmed by AFM and SIMS. The obvious large forward current at a small voltage bias for the sample annealed at 150 mJ/cm^2 implies the large generation–recombination current due to the unhealed implantation damage. The I_{on}/I_{off} ratio up to 1.99×10^5 is achieved at a laser energy density at 250 mJ/cm^2, which is one or two orders of magnitude higher than those shown in the previous reports.[16,19,28] Those results suggest that the Ge n$^+$/p shallow junction with high electrical performance can be achieved by excimer laser annealing and phosphorus implantation into p-type Ge at a relatively low laser energy density.

In summary, the influence of laser energy density on dopant diffusion and recrystallization of phosphorus-implanted Ge has been investigated utilizing 248 nm KrF

excimer laser annealing. A low specific contact resistivity of $1.61 \times 10^{-6}\,\Omega\cdot\mathrm{cm}^2$ for Al/n^+Ge ohmic contact and a well-behaved Ge n^+/p shallow junction diode with a rectification ratio up to 1.99×10^5 are obtained after excimer laser annealing of phosphorus-implanted Ge at $250\,\mathrm{mJ/cm}^2$. Therefore, ultrashallow n^+/p junctions for Ge with higher rectification ratio are feasible by scaling down the P ion implant energy and the laser annealing fluence, which would be immensely beneficial to the nanoscaled Ge MOSFET applications.

Acknowledgments This work was supported by the National Basic Research Program of China under grant Nos. 2012CB933503 and 2013CB632103, the National Natural Science Foundation of China under grant Nos. 61176092, 61036003, and 60837001, Ph. D. Programs Foundation of the Ministry of Education of China under grant No. 20110121110025, and the Fundamental Research Funds for the Central Universities under grant No. 2010121056.

1) D. Lee, S. Raghunathan, R. J. Wilson, D. E. Nikonov, K. Saraswat, and S. X. Wang: Appl. Phys. Lett. **96** (2010) 052514.
2) S. J. Whang, S. J. Lee, F. Gao, N. Wan, C. X. Zhu, J. S. Pan, L. J. Tang, and D. L. Kwong: IEDM Tech. Dig., 2004, p. 307.
3) A. Dimoulas, P. Tsipas, A. Sotiropoulos, and E. K. Evangelou: Appl. Phys. Lett. **89** (2006) 252110.
4) Z. Wu, W. Huang, C. Li, H. Lai, and S. Chen: IEEE Trans. Electron Devices **59** (2012) 1328.
5) M. Koike, Y. Kamata, T. Ino, D. Hagishima, K. Tatsumura, M. Koyama, and A. Nishiyama: J. Appl. Phys. **104** (2008) 023523.
6) V. P. Markevich, I. D. Hawkins, A. R. Peaker, K. V. Emtsev, V. V. Emtsev, V. V. Litvinov, L. I. Murin, and L. Dobaczewski: Phys. Rev. B **70** (2004) 235213.
7) D. Kuzum, T. Krishnamohan, A. Nainani, Y. Sun, P. A. Pianetta, H.-S. P. Wong, and K. C. Saraswat: IEDM Tech. Dig., 2009, p. 453.
8) C. O. Chui, L. Kulig, J. Moran, W. Tsai, and K. C. Saraswat: Appl. Phys. Lett. **87** (2005) 091909.
9) C. Wündisch, M. Posselt, B. Schmidt, V. Heera, T. Schumann, A. Mücklich, R. Grötzschel, W. Skorupa, T. Clarysse, E. Simoen, and H. Hortenbach: Appl. Phys. Lett. **95** (2009) 252107.
10) H.-Y. Yu, S.-L. Cheng, P. B. Griffin, Y. Nishi, and K. C. Saraswat: IEEE Electron Device Lett. **30** (2009) 1002.
11) S. Huang, C. Li, C. Chen, C. Wang, G. Yan, H. Lai, and S. Chen: Appl. Phys. Lett. **102** (2013) 182102.
12) K. Martens, R. Rooyackers, A. Firrincieli, B. Vincent, R. Loo, B. De Jaeger, M. Meuris, P. Favia, H. Bender, B. Douhard, W. Vandervorst, E. Simoen, M. Jurczak, D. J. Wouters, and J. A. Kittl: Appl. Phys. Lett. **98** (2011) 013504.
13) Z. Wu, C. Wang, W. Huang, C. Li, H. Lai, and S. Chen: ECS J. Solid State Sci. Technol. **1** (2012) P30.
14) J. Oh, I. Ok, C.-Y. Kang, M. Jamil, S.-H. Lee, W.-Y. Loh, J. Huang, B. Sassman, L. Smith, S. Parthasarathy, B. E. Coss, W.-H. Choi, H.-D. Lee, M. Cho, S. K. Banerjee, P. Majhi, P. D. Kirsch, H.-H. Tseng, and R. Jammy: IEEE VLSI Tech. Dig., 2009, p. 238.
15) B. Yu, Y. Wang, H. Wang, Q. Xiang, C. Riccobene, S. Talwar, and M.-R. Lin: IEDM Tech. Dig., 1999, p. 509.
16) G. Thareja, S. Chopra, B. Adamas, Y. Kim, S. Moffatt, K. Saraswat, and K. Saraswat: IEEE Electron Device Lett. **32** (2011) 838.
17) K. Martens, A. Firrincieli, R. Rooyackers, B. Vincent, R. Loo, S. Locorotondo, E. Rosseel, T. Vandeweyer, G. Hellings, B. De Jaeger, M. Meuris, P. Favia, H. Bender, B. Douhard, J. Delmotte, W. Vandervorst, E. Simoen, G. Jurczak, D. Wouters, and J. A. Kittl: IEDM Tech. Dig., 2010, p. 428.
18) A. Firrincieli, K. Martens, R. Rooyackers, B. Vincent, E. Rosseel, E. Simoen, J. Geypen, H. Bender, C. Claeys, and J. A. Kittl: Appl. Phys. Lett. **99** (2011) 242104.
19) J. Huang, N. Wu, Q. Zhang, C. Zhu, A. A. O. Tay, G. Chen, and M. Hong: Appl. Phys. Lett. **87** (2005) 173507.
20) C. O. Chui, K. Gopalakrishnan, P. B. Griffin, J. D. Plummer, and K. C. Saraswat: Appl. Phys. Lett. **83** (2003) 3275.
21) E. Simoen, A. Satta, A. D'Amore, T. Janssens, T. Clarysse, K. Martens, B. De Jaeger, A. Benedetti, I. Hoflijk, B. Brijs, M. Meuris, and W. Vandervorst: Mater. Sci. Semicond. Process. **9** (2006) 634.
22) C. H. Poon, L. S. Tan, B. J. Cho, and A. Y. Du: J. Electrochem. Soc. **152** (2005) G895.
23) H. Shang, K.-L. Lee, P. Kozlowski, C. D'Emic, I. Babich, E. Sikorski, M. Ieong, H.-S. P. Wong, K. Guarini, and W. Haensch: IEEE Electron Device Lett. **25** (2004) 135.
24) E. Simoen and J. Vanhellemont: J. Appl. Phys. **106** (2009) 103516.
25) D. B. Cuttriss: Bell Syst. Tech. J. **40** (1961) 509.
26) S. Koffel, A. Claverie, G. BenAssayag, and P. Scheiblin: Mater. Sci. Semicond. Process. **9** (2006) 664.
27) A. Claverie, C. Vieu, J. Fauré, and J. Beauvillain: J. Appl. Phys. **64** (1988) 4415.
28) W. B. Chen, B. S. Shie, and A. Chin: IEEE Electron Device Lett. **32** (2011) 449.